







Finding Direct-collapse Black Holes at Birth

Daniel J. Whalen^{1,2} , Marco Surace¹, Carla Bernhardt³, Erik Zackrisson⁴ , Fabio Pacucci^{5,6} , Bodo Ziegler⁷, and Michaela Hirschmann⁸ 

¹ Institute of Cosmology and Gravitation, University of Portsmouth, Portsmouth PO1 3FX, UK; daniel.whalen@port.ac.uk

² Ida Pfeiffer Professor, University of Vienna, Department of Astrophysics, Tuerkenschanzstrasse 17, A-1180, Vienna, Austria

³ Universität Heidelberg, Institut für Theoretische Astrophysik, Albert-Ueberle-Str. 2, D-69120 Heidelberg, Germany

⁴ Observational Astrophysics, Department of Physics and Astronomy, Uppsala University, Box 516, SE-751 20 Uppsala, Sweden

⁵ Black Hole Initiative, Harvard University, Cambridge, MA 02138, USA

⁶ Center for Astrophysics | Harvard & Smithsonian, Cambridge, MA 02138, USA

⁷ University of Vienna, Department of Astrophysics, Tuerkenschanzstrasse 17, A-1180, Vienna, Austria

⁸ DARK, Niels Bohr Institute, University of Copenhagen, Lyngbyvej 2, DK-2100 Copenhagen, Denmark

Received 2020 May 2; revised 2020 June 10; accepted 2020 June 16; published 2020 July 3

Abstract

Direct-collapse black holes (DCBHs) are currently one of the leading contenders for the origins of the first quasars in the universe, over 300 of which have now been found at $z > 6$. But the birth of a DCBH in an atomically cooling halo does not by itself guarantee it will become a quasar by $z \sim 7$, the halo must also be located in cold accretion flows or later merge with a series of other gas-rich halos capable of fueling the BH's rapid growth. Here, we present near-infrared luminosities for DCBHs born in cold accretion flows in which they are destined to grow to $10^9 M_\odot$ by $z \sim 7$. Our observables, which are derived from cosmological simulations with radiation hydrodynamics with Enzo, reveal that DCBHs could be found by the James Webb Space Telescope at $z \lesssim 20$ and strongly lensed DCBHs might be found in future wide-field surveys by Euclid and the Wide-Field Infrared Space Telescope at $z \lesssim 15$.

Unified Astronomy Thesaurus concepts: [Intermediate-mass black holes \(816\)](#); [Supermassive black holes \(1663\)](#); [Quasars \(1319\)](#); [Population III stars \(1285\)](#); [Primordial galaxies \(1293\)](#); [High-redshift galaxies \(734\)](#)

1. Introduction

Direct-collapse black holes (DCBHs) may be the origins of the first quasars in the universe (e.g., Mortlock et al. 2011; Bañados et al. 2018; Matsuoka et al. 2019). They are thought to form in primordial halos immersed in either strong Lyman–Werner (LW) UV fluxes or highly supersonic baryon streaming flows, either of which can prevent them from forming primordial (or Population III) stars until they reach masses of 10^7 – $10^8 M_\odot$ and virial temperatures of $\sim 10^4$ K that trigger rapid atomic H cooling (Inayoshi et al. 2019; Smith & Bromm 2019). Atomic cooling causes gas to collapse at rates of up to $\sim 1 M_\odot \text{ yr}^{-1}$, forming an accretion disk that builds up a single, supermassive star at its center (e.g., Regan & Haehnelt 2009; Latif et al. 2013—although binaries or even small multiples are now thought to be possible; Latif et al. 2020).

Stellar evolution models show that these stars can reach masses of a few $10^5 M_\odot$ before collapsing to DCBHs via the general relativistic instability (Umeda et al. 2016; Woods et al. 2017; Haemmerlé et al. 2018a, 2018b), although a few for which accretion has shut down have been found to explode as highly energetic thermonuclear supernovae (Johnson et al. 2013a; Whalen et al. 2013a, 2013b; Chen et al. 2014). DCBHs are currently the leading candidates for the seeds of the first supermassive black holes (SMBHs) because they are born with large masses in high densities in halos that can retain their fuel supply, even when heated by X-rays (Johnson et al. 2013b; see Valiante et al. 2017; Woods et al. 2019 for recent reviews). In contrast, while Population III star BHs in principle can reach $10^9 M_\odot$ with periodic episodes of super- or hyper-Eddington accretion (Volonteri et al. 2015; Pezzulli et al. 2016), their

environments are hostile to such growth (Whalen et al. 2004; Whalen & Fryer 2012; Smith et al. 2018).

The formation of a DCBH does not guarantee it will become a $10^9 M_\odot$ quasar by $z > 6$ because a large gas reservoir is also needed for its sustained growth. Its host halo must either lie at the nexus of cold accretion flows (e.g., Di Matteo et al. 2012; Yue et al. 2014) or undergo a series of mergers with other gas-rich halos capable of fueling its rapid growth (e.g., Li et al. 2007). Atomically cooled halos fed by cold streams are more turbulent than other halos because they can reach masses greater than $10^{12} M_\odot$ by $z \sim 7$ (Smidt et al. 2018). DCBHs born in such environments can thus grow more rapidly than in other halos.

What are the prospects for detecting DCBHs, and thus the birth of the first quasars? Using one-dimensional (1D) radiation hydrodynamical models, Pacucci et al. (2015) predicted that DCBHs could be detected by the James Webb Space Telescope (JWST) in the near-infrared (NIR) at $z \sim 25$ and by the Advanced Telescope for High-Energy Astrophysics (ATHENA) at $z \sim 15$. Natarajan et al. (2017) used such models to develop criteria for distinguishing the host galaxies of DCBHs from those of other SMBH seeds at $z \sim 10$, showing that JWST can distinguish between seeding mechanisms at this redshift. Barrow et al. (2018) post-processed cosmological simulations of DCBH birth in atomically cooling halos with Monte Carlo radiative transfer to produce synthetic BH spectra. Their models included X-rays from the BH and star formation and supernova feedback in its host halo. They found similar limits for DCBH detections in the NIR as Pacucci et al. (2015) and Natarajan et al. (2017) with some spectral differences owing in part to star formation in their halo.

But these models either assume idealized halo profiles or halos that are not fed by cold streams or later grow to large

masses. Like the supermassive stars from which they form, DCBHs are deeply imbedded in these flows, which can heavily reprocess radiation from the BH in ways that have not been considered in previous studies, changing their rest-frame spectra and NIR luminosities today (see also Ge & Wise 2017; Smith et al. 2017; Wolcott-Green et al. 2020 for how radiative transfer effects deep in these halos can affect the dynamics of their flows). Here, we calculate NIR AB magnitudes for a DCBH at birth in the flows in which it grows into a quasar by $z \sim 7$. Rather than assuming a grid of accretion rates for the BH, ours are an emergent feature of a cosmological simulation. Our models capture the anisotropy of X-ray breakout into the early intergalactic medium (IGM) and how it affects their detection today. In Section 2 we describe our calculations and examine DCBH spectra and AB magnitudes for a variety of JWST, Euclid, and Wide-Field Infrared Survey Telescope (WFIRST) bands in Section 3. We conclude in Section 4.

2. Numerical Method

We first extract luminosities and H II region profiles for the DCBH from Smidt et al. (2018), which was done with the Enzo adaptive mesh refinement (AMR) cosmology code (Bryan et al. 2014). They are then post-processed with Cloudy (Ferland et al. 2017) to obtain rest-frame BH spectra. These spectra are then cosmologically redshifted and dimmed, corrected by absorption by the neutral IGM at $z > 6$, and convolved with telescope filter functions to compute AB magnitudes in a variety of NIR bands as a function of source redshift.

2.1. Enzo Model

In the Smidt et al. (2018) Enzo simulation, a halo in a $100 h^{-1} \text{Mpc}$ box reaches a mass of $3 \times 10^8 M_{\odot}$ at $z = 19.2$ and begins to atomically cool. At this redshift X-rays from a $10^5 M_{\odot}$ DCBH are turned on in the halo, which later grows to $1.2 \times 10^{12} M_{\odot}$ by $z = 7.1$ by accretion rather than major mergers. The X-rays were propagated with MORAY (Wise & Abel 2011), which is self-consistently coupled to hydrodynamics and nine-species nonequilibrium primordial gas chemistry in Enzo. The simulation included radiation pressure on gas due to photoionizations, Compton heating by X-rays, and primordial gas cooling.

A maximum of 10 levels of adaptive mesh refinement produced a resolution of 35 pc (comoving), which was sufficient to resolve the gas flows and radiation transport deep in the halo. The DCBH was represented by a sink particle with 1 keV X-rays and an alpha disk model for accretion rates to approximate the transport of angular momentum out of the disk on subgrid scales. Although Population II and III star formation, stellar winds, and ionizing UV and supernovae due to stars were turned on at the same time as X-rays from the BH, no stars formed in the short times we examine the DCBH here so its host halo is still free of metals. An image of the H II region of the DCBH at $z = 17$ is shown in the right panel of Figure 1.

2.2. Cloudy Spectra

To compute DCBH spectra we port spherically averaged density and temperature profiles of the H II region of the BH from Enzo to Cloudy. They are tabulated in 33 bins that are uniformly partitioned in log radius and extend to the outer layers of the H II region where the temperature of the gas has

fallen below 10^4 K ($\sim 30 \text{ kpc}$). Each radial bin, or shell, constitutes a single Cloudy model in which densities and temperatures are assumed to be constant. The spectrum emerging from the outer surface of one shell is calculated and then used as the incident spectrum of the next shell. The spectrum emerging from the outermost shell of the H II region is taken to be the rest-frame spectrum of the quasar. Although our 1D profiles smooth out anisotropies in angle due to cosmological structures, they capture their average effects on AB magnitudes. The actual magnitudes could be brighter along some lines of sight than others because of these anisotropies.

We apply the default Cloudy broken power-law spectrum to the lower face of the innermost shell because of its similarity to that used in Pacucci et al. (2015), where $F_{\nu} \propto \nu^{\alpha}$ and $\alpha = -2$ for $h\nu > 50 \text{ keV}$ ($2.48 \times 10^{-5} \mu\text{m}$), $\alpha = -1.6$ for $50 \text{ keV} > h\nu > 0.124 \text{ eV}$ ($10 \mu\text{m}$), and $\alpha = 5/2$ above $10 \mu\text{m}$. It is normalized to the bolometric luminosity of the DCBH. Coronal equilibrium is assumed, in which the gas is collisionally ionized. We require Cloudy to use the temperatures Enzo calculates for the H II region instead of inferring them from the spectrum and luminosity of the BH and its surrounding density field because they take into account cooling due to nonequilibrium primordial gas chemistry in cosmological flows. How we compute AB magnitudes from rest-frame Cloudy spectra is described in detail in Surace et al. (2018).

3. Detecting DCBHs

We show rest-frame spectra for the DCBH at $z = 19$ before and after reprocessing by the halo in the left panel of Figure 1. It has a bolometric luminosity of $2.42 \times 10^{44} \text{ erg s}^{-1}$ corresponding to an accretion rate of $0.85 L_{\text{Edd}}$. There is a conspicuous lack of metal lines in the emergent spectrum because X-rays from the BH have not yet triggered star formation. Strong Ly α absorption is evident at 1216 \AA as is continuum absorption below 912 \AA due to the ionization of H. Additional absorption features due to ionization of He I and He II are visible at 504 \AA and 227 \AA , respectively. Several prominent He emission lines are superimposed on the continuum absorption below 912 \AA . There are H α and weak Paschen series lines at 6560 \AA and 12800 \AA . Unlike the spectrum of the cool, red progenitor star (Surace et al. 2018), there is a lack of continuum absorption above and below 16500 \AA due to H $^{-}$ bound-bound and bound-free opacity in the DCBH spectrum because it is destroyed by radiation from the BH.

3.1. NIR Magnitudes

We show AB magnitudes for the DCBH at $z = 8-20$ in JWST Near Infrared Camera (NIRCam) bands at $2.5-4.6 \mu\text{m}$ along with 5σ detection limits for the filters for 100 hr exposures in the top left panel of Figure 2. The BH is clearly brighter in the NIR than its progenitor star (see Figures 13, 4, and 3 of Hosokawa et al. 2013; Surace et al. 2018; Surace et al. 2019, respectively), with AB magnitudes that are 0.5–2.5 brighter depending on filter and wavelength. The magnitudes in all four filters are also more tightly grouped together in consequence of the relatively flat power-law spectrum of the BH. The drop in magnitude at $z = 18$ at $2.5 \mu\text{m}$ is due to the redshifting of the Ly α absorption feature of the rest-frame spectrum into that wavelength. The BH is brightest in the

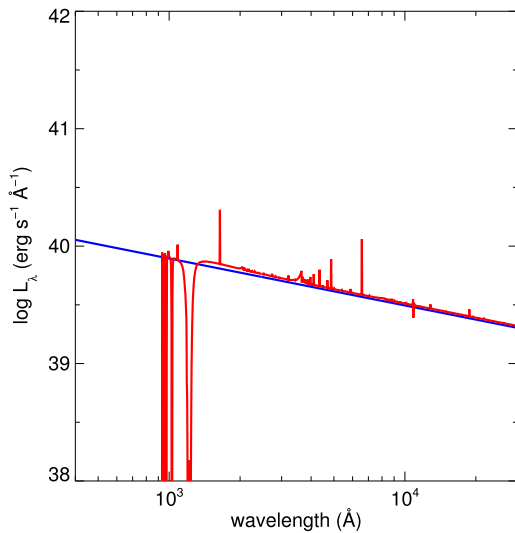


Figure 1. Birth of a DCBH at $z = 19$. Left panel: rest-frame spectra for the DCBH at $z = 19$ before (blue) and after (red) reprocessing by its host halo. Right panel: ionized H fractions in the vicinity of the BH at $z = 17$. The image is 30 kpc proper on a side.

4.60 μm and 4.44 μm filters over all redshifts, with magnitudes that vary from 27.5–30.1 from $z = 8$ –20. We find that detections in all four NIRCcam filters are possible out to $z \sim 19$ with 100 hr exposures and in all the bands redward of 3.56 μm out to $z \sim 25$.

As shown in the top right panel of Figure 2, DCBH magnitudes in the JWST Mid-Infrared Instrument (MIRI) filters are significantly brighter than in NIRCcam, ranging from 24.5–27 at 25.5 μm to 27–29.8 at 5.6 μm for $z = 8$ –20. Some of these magnitudes are also much brighter than those of the progenitor star. For example, the magnitudes of a red supermassive star (SMS) vary from 31–32 at 5.6 μm over the same redshift range (Surace et al. 2018). The ordering of the magnitudes with filter wavelength for the SMS is opposite that of the DCBH, with the shortest wavelengths having the brightest magnitudes. This feature is due to continuum absorption by H^- in the envelope of the SMS that is absent from the host halo of the BH. However, while the DCBH magnitudes are brighter in MIRI than NIRCcam, the 5σ detection limits for a 100 hr exposure are considerably dimmer, ranging from 24.8 at 18 μm to 28.0 at 5.6 μm . They limit detections of DCBHs to $z = 9$ at 18 μm to $z = 12$ at 5.6 μm . Nevertheless, these AB magnitudes reveal that MIRI could be a powerful instrument for the detection of DCBHs at high redshifts and could discriminate them from SMSs at the same epochs, for which there would be no MIRI signal.

We show DCBH magnitudes in the Euclid and WFIRST bands in the bottom two panels of Figure 2. Absorption by the neutral IGM at $z \gtrsim 6$ quenches flux in the Y, J, and H bands at $z \gtrsim 7$, 10, and 14, respectively, limiting DCBH detections to these redshifts in these filters. Magnitudes vary from 29 to 34 in Euclid and 29–37 in WFIRST. The AB magnitude limits of 26 and 28 for surveys currently planned for Euclid and WFIRST, respectively, would rule out direct detections of DCBHs at $z \gtrsim 6$ –8. We also computed AB magnitudes for all four cases with the spectrum for the $1 \times 10^5 M_\odot$ DCBH used in Pacucci et al. (2015) and found virtually no differences with those derived from our power-law spectrum.

3.2. DCBH Formation/Detection Rates

While our synthetic spectrum indicates that DCBHs would be detectable in multiband photometric surveys with JWST at $z \sim 8$ –20, the prospect of actually finding such objects in a given survey depends on their formation rates and the time interval over which a DCBH is likely to display tell-tale spectral or photometric signatures. Wise et al. (2019) and Regan et al. (2020) identified atomically cooling halos at $z \gtrsim 12$ in the Renaissance simulations that could form DCBHs. The three DCBH candidate halos that appeared in their 220 cMpc^3 average-density region over the ~ 70 Myr from $z \sim 14$ to 12 imply a formation rate of $\sim 10^{-10} \text{ cMpc}^{-3} \text{ yr}^{-1}$ at these redshifts. While their simulations did not track the subsequent evolution of the gas in these halos, this formation rate can be used to place an upper limit on detections of DCBHs in future JWST surveys.

If we adopt a characteristic timescale of 10^7 yr for the validity of our spectrum (set by when star formation likely begins in its host halo) then we expect a comoving density of observable DCBHs of $\sim 10^{-3} f_{\text{DCBH}} \text{ cMpc}^{-3}$, where f_{DCBH} is the fraction of candidate halos that produce $\sim 10^5 M_\odot$ BHs. The JWST NIRCcam field of view (9.7 arcmin^2) covers $1.3 \times 10^4 \text{ cMpc}^3$ per unit redshift at $z \sim 12$, so one would expect $\sim 10 f_{\text{DCBH}}$ detectable DCBHs for each such survey field. With planned medium-deep NIRCcam multiband surveys covering ~ 20 times this area down to AB mag 29 in the longest-wavelength NIRCcam filters (Rieke et al. 2019), the prospects for detecting DCBHs photometrically with JWST would appear to be quite good, even if just some minor fraction ($f_{\text{DCBH}} \gtrsim 0.01$) of the Regan et al. (2020) candidate halos end up forming them. Another route to detection could be to search the field around an unusually bright $z \sim 15$ galaxy found by some other means, as Wise et al. (2019) and Regan et al. (2020) note that the formation rate of DCBHs may rise by more than an order of magnitude in high-density regions, where the most massive first galaxies are also expected to form.

4. Discussion and Conclusion

With NIRCcam AB mag photometry limits of 31–32 and NIRSspec limits of ~ 29 , JWST will be able to detect the birth

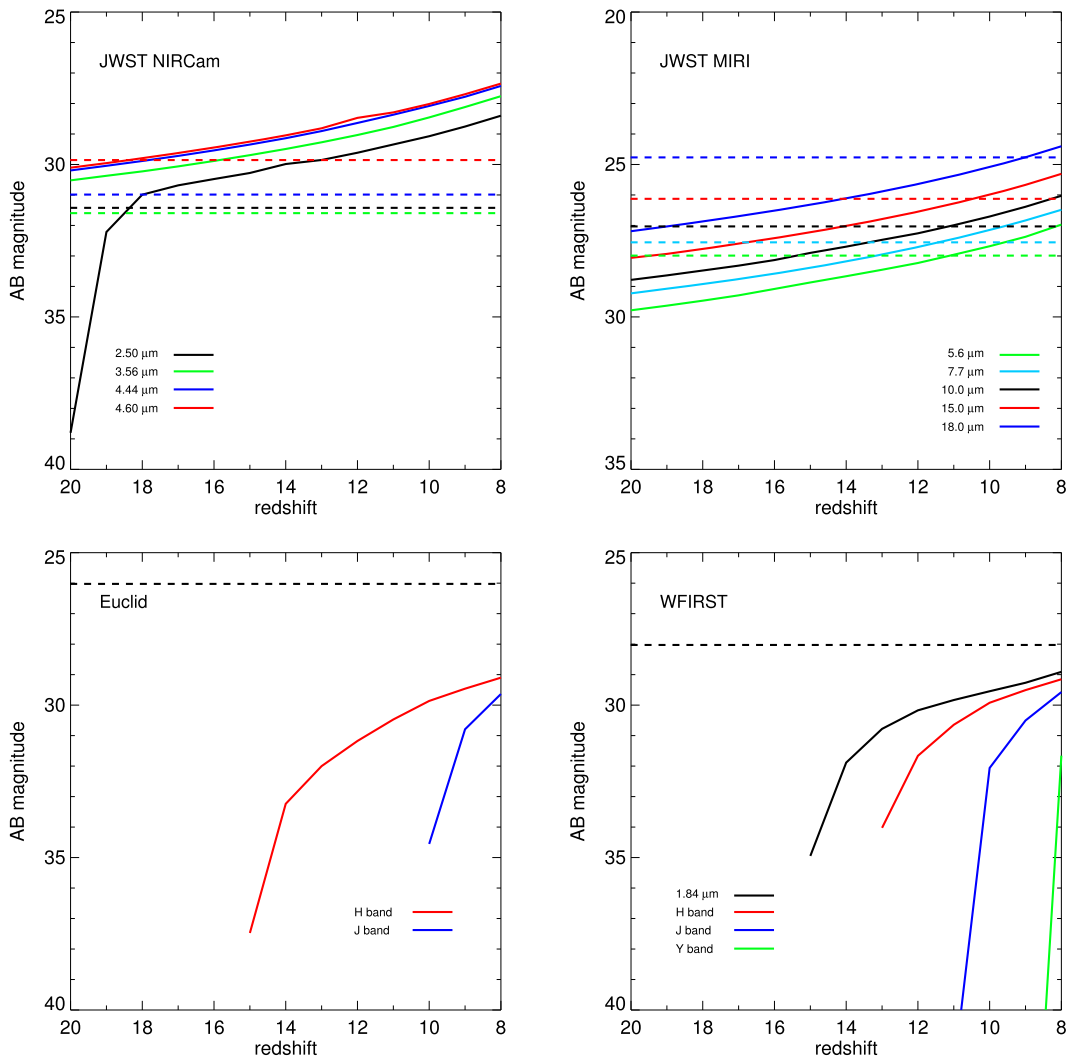


Figure 2. NIR AB magnitudes for the $1.0 \times 10^5 M_{\odot}$ DCBH at birth as it would appear at $z = 8-20$ in JWST, Euclid, and WFIRST. Top left: JWST NIRCam bands. The horizontal dashed lines are 5σ AB magnitude detection limits for 100 hour exposures in the filters of corresponding color (2.50 μm : 31.4 mag, 3.56 μm : 31.5 mag, 4.44 μm : 31.0 mag, and 4.60 μm : 29.8 mag). Top right: JWST MIRI bands. The horizontal dashed lines are 5σ AB magnitude detection limits for 100 hr exposures in the filters of corresponding color (5.6 μm : 28.0 mag, 7.7 μm : 27.6 mag, 10.0 μm : 27.0 mag, 15.0 μm : 26.1 mag, and 18.0 μm : 24.7 mag). Bottom left: Euclid. Bottom right: WFIRST. The horizontal dashed lines in the bottom panels are detection limits for deep-drilling fields in Euclid and WFIRST (26 mag and 28 mag, respectively).

of the first quasars at $z \gtrsim 20$ and spectroscopically confirm their redshift out to $z \sim 10-12$. Our DCBH magnitudes are consistent with simplified 1D calculations in past studies (Yue et al. 2013; Pacucci et al. 2015; Natarajan et al. 2017). As shown in the previous section, up to 10 DCBHs could appear in any given JWST survey field from $z = 8$ to 20. But the prospects for discovering them would be better if they could also be found by Euclid and WFIRST because their wide fields would enclose far more of them at high redshifts. Once flagged, DCBH candidates could then be examined with JWST or ground-based extremely large telescopes in greater detail. But, as shown in Figure 2, DCBH magnitudes in the H-band magnitudes at $z = 8-20$ are dimmer than the detection limits currently envisioned for Euclid and WFIRST (26 and 28, respectively). In principle, these magnitudes could become brighter if accretion rates exceed the Eddington limit but only modestly so because the luminosity rises only logarithmically with such rates, not linearly.

However, this does not mean Euclid and WFIRST cannot find DCBHs at birth because only modest gravitational lensing





is required to boost their fluxes above their detection limits. The survey areas of both missions will enclose thousands of galaxy clusters and massive galaxies that could lens flux from background DCBHs, and at $z \sim 8-14$ magnification factors of only 10–100 would be required to reveal them. It is likely that a sufficient fraction of their survey areas will be magnified by such factors (Pacucci & Loeb 2019; Rydberg et al. 2020). Even higher magnifications may be realized in future surveys of individual cluster lenses by JWST but at the cost of smaller lensing volumes (e.g., Whalen et al. 2013c; Windhorst et al. 2018).

As discussed earlier, the host halo of our DCBH is constantly replenished by new gas from cold accretion flows, in contrast to most other atomically cooled halos at high redshift. The lower average densities of those halos would have less effect on the emergent spectrum of the BH and they would therefore have somewhat lower fluxes in the NIR. DCBHs in general can be distinguished from their SMS progenitors at high redshift because they are brighter and have much higher ratios of flux in the MIRI and NIRCam bands. Natarajan et al.

(2017) found that DCBHs can be readily distinguished from early galaxies at similar redshifts in color–color space, which would also be true for our models because of the similarities in source spectra of both studies (see also Valiante et al. 2018). Also, unlike SMSs and high- z galaxies, they are transients because of variations in cosmological flows onto them on timescales as short as the redshifted light-crossing time of the BH. Periodic dimming and brightening could therefore tag these objects as high- z BHs in transient surveys with well-chosen cadences proposed for JWST such as FLARE (Wang et al. 2017). Synergies between Euclid or WFIRST and JWST or 20 + m ground-based telescopes could open the era of $z = 8$ –20 quasar astronomy in the coming decade.

The authors thank the anonymous referee for constructive comments that improved the quality of this Letter. D.J.W. was supported by the Ida Pfeiffer Professorship at the Institute of Astrophysics at the University of Vienna and by STFC New Applicant Grant ST/P000509/1. E.Z. acknowledges funding from the Swedish National Space Board. F.P. acknowledges support from a Clay Fellowship administered by the Smithsonian Astrophysical Observatory and from the black hole Initiative at Harvard University, which is funded by grants from the John Templeton Foundation and the Gordon and Betty Moore Foundation. M.H. acknowledges financial support from the Carlsberg Foundation via a Semper Ardens grant (CF15-0384). Our simulations were performed on the Sciama cluster at the Institute of Cosmology and Gravitation at the University of Portsmouth. We also acknowledge support by the state of Baden–Württemberg through bwHPC (the bwForCluster).

ORCID iDs

Daniel J. Whalen  <https://orcid.org/0000-0001-6646-2337>
 Erik Zackrisson  <https://orcid.org/0000-0003-1096-2636>
 Fabio Pacucci  <https://orcid.org/0000-0001-9879-7780>
 Michaela Hirschmann  <https://orcid.org/0000-0002-3301-3321>

References

Bañados, E., Venemans, B. P., Mazzucchelli, C., et al. 2018, *Natur*, **553**, 473
 Barrow, K. S. S., Aykutaalp, A., & Wise, J. H. 2018, *NatAs*, **2**, 987
 Bryan, G. L., Norman, M. L., O’Shea, B. W., et al. 2014, *ApJS*, **211**, 19
 Chen, K.-J., Heger, A., Woosley, S., et al. 2014, *ApJ*, **790**, 162
 Di Matteo, T., Khandai, N., DeGraf, C., et al. 2012, *ApJL*, **745**, L29

Ferland, G. J., Chatzikos, M., Guzmán, F., et al. 2017, *RMxAA*, **53**, 385
 Ge, Q., & Wise, J. H. 2017, *MNRAS*, **472**, 2773
 Haemmerlé, L., Woods, T. E., Klessen, R. S., Heger, A., & Whalen, D. J. 2018a, *ApJL*, **853**, L3
 Haemmerlé, L., Woods, T. E., Klessen, R. S., Heger, A., & Whalen, D. J. 2018b, *MNRAS*, **474**, 2757
 Hosokawa, T., Yorke, H. W., Inayoshi, K., Omukai, K., & Yoshida, N. 2013, *ApJ*, **778**, 178
 Inayoshi, K., Visbal, E., & Haiman, Z. 2019, arXiv:1911.05791
 Johnson, J. L., Whalen, D. J., Even, W., et al. 2013a, *ApJ*, **775**, 107
 Johnson, J. L., Whalen, D. J., Li, H., & Holz, D. E. 2013b, *ApJ*, **771**, 116
 Latif, M. A., Khochfar, S., & Whalen, D. 2020, *ApJL*, **892**, L4
 Latif, M. A., Schleicher, D. R. G., Schmidt, W., & Niemeyer, J. 2013, *MNRAS*, **430**, 588
 Li, Y., Hernquist, L., Robertson, B., et al. 2007, *ApJ*, **665**, 187
 Matsuoka, Y., Onoue, M., Kashikawa, N., et al. 2019, *ApJL*, **872**, L2
 Mortlock, D. J., Warren, S. J., Venemans, B. P., et al. 2011, *Natur*, **474**, 616
 Natarajan, P., Pacucci, F., Ferrara, A., et al. 2017, *ApJ*, **838**, 117
 Pacucci, F., Ferrara, A., Volonteri, M., & Dubus, G. 2015, *MNRAS*, **454**, 3771
 Pacucci, F., & Loeb, A. 2019, *ApJL*, **870**, L12
 Pezzulli, E., Valiante, R., & Schneider, R. 2016, *MNRAS*, **458**, 3047
 Regan, J. A., & Haehnelt, M. G. 2009, *MNRAS*, **396**, 343
 Regan, J. A., Wise, J. H., O’Shea, B. W., & Norman, M. L. 2020, *MNRAS*, **492**, 3021
 Rieke, M., Arribas, S., Bunker, A., et al. 2019, *BAAS*, **51**, 45
 Rydberg, C.-E., Whalen, D. J., Maturi, M., et al. 2020, *MNRAS*, **491**, 2447
 Smidt, J., Whalen, D. J., Johnson, J. L., Surace, M., & Li, H. 2018, *ApJ*, **865**, 126
 Smith, A., Becerra, F., Bromm, V., & Hernquist, L. 2017, *MNRAS*, **472**, 205
 Smith, A., & Bromm, V. 2019, *ConPh*, **60**, 111
 Smith, B. D., Regan, J. A., Downes, T. P., et al. 2018, *MNRAS*, **480**, 3762
 Surace, M., Zackrisson, E., Whalen, D. J., et al. 2019, *MNRAS*, **488**, 3995
 Surace, M., Whalen, D. J., Hartwig, T., et al. 2018, *ApJL*, **869**, L39
 Umeda, H., Hosokawa, T., Omukai, K., & Yoshida, N. 2016, *ApJL*, **830**, L34
 Valiante, R., Agarwal, B., Habouzit, M., & Pezzulli, E. 2017, *PASA*, **34**, e031
 Valiante, R., Schneider, R., Zappacosta, L., et al. 2018, *MNRAS*, **476**, 407
 Volonteri, M., Silk, J., & Dubus, G. 2015, *ApJ*, **804**, 148
 Wang, L., Baade, D., Baron, E., et al. 2017, arXiv:1710.07005
 Whalen, D., Abel, T., & Norman, M. L. 2004, *ApJ*, **610**, 14
 Whalen, D. J., & Fryer, C. L. 2012, *ApJL*, **756**, L19
 Whalen, D. J., Johnson, J. L., Smidt, J., et al. 2013a, *ApJ*, **777**, 99
 Whalen, D. J., Johnson, J. L., Smidt, J., et al. 2013b, *ApJ*, **774**, 64
 Whalen, D. J., Smidt, J., Johnson, J. L., et al. 2013c, arXiv:1312.6330
 Windhorst, R. A., Timmes, F. X., Wylie, J. S. B., et al. 2018, *ApJS*, **234**, 41
 Wise, J. H., & Abel, T. 2011, *MNRAS*, **414**, 3458
 Wise, J. H., Regan, J. A., O’Shea, B. W., et al. 2019, *Natur*, **566**, 85
 Wolcott-Green, J., Haiman, Z., & Bryan, G. L. 2020, arXiv:2001.05498
 Woods, T. E., Agarwal, B., Bromm, V., et al. 2019, *PASA*, **36**, e027
 Woods, T. E., Heger, A., Whalen, D. J., Haemmerlé, L., & Klessen, R. S. 2017, *ApJL*, **842**, L6
 Yue, B., Ferrara, A., Salvaterra, R., Xu, Y., & Chen, X. 2013, *MNRAS*, **433**, 1556
 Yue, B., Ferrara, A., Salvaterra, R., Xu, Y., & Chen, X. 2014, *MNRAS*, **440**, 1263